Methods

Here we provide details of SOFIA/FIFI-LS observations combined with Herschel/PACS archival data of the FIR fine structure lines of five luminous infrared galaxies (ULIRGs) with $S_{60\mu m} \geq 7$ Jy at $0.035 < z < 0.075$ (§ 1 and § 2). We then present some details about FIR-based metallicity measurements (§ 3) and stellar masses as well as optical-based metallicity measurements used in this work (§ 4). Throughout this paper we adopt a Chabrier[46] initial mass function (IMF), and the concordance ΛCDM cosmology[47] with $\Omega_{\rm m} = 0.3$, $\Omega_{\Lambda} = 0.7$, and H_0 = 70 km s^{-1} Mpc^{-1}.

1 The sample of Ultra Luminous Infrared Galaxies

The Herschel ULIRG Survey (HERUS[53]) and Survey with Herschel of the ISM in Nearby INfrared Galaxies (SHINING[48–50], overlapping with ULIRGs in the Great Observatories All-Sky LIRG Survey (GOALS) sample[51]), assembled Herschel/PACS and SPIRE observations of 43 ULIRGs at $z < 0.27$ drawn from the IRAS PSC-z survey[52], with a 60 μm flux density greater than ~ 1.7Jy, and made detailed diagnostics of the FIR fine structure lines possible[48,53,54]. All objects have been spectroscopically confirmed with high-resolution optical observations and observed with Spitzer IRS for mid-IR lines and PAH features[55–57].

Although HERUS, SHINING, and GOALS surveys already represent the best-explored samples so far with some FIR lines observed such as [OI]63 μm and [CII]158 μm, none of the objects have the complete set of lines simultaneously observed, missing critical set of lines [OIII]52 μm, [NIII]57 μm and [OIII]88 for the study on metal abundances reported in the Letter to the Editor. These three emission lines are crucial since it has been shown that the flux line ratio of (2.2$\times$[OIII]88+[OIII]52)/[NIII]57 provides a powerful tool for gas-phase metallicity of galaxies, especially for highly obscured star-forming galaxies[54].

Among these three lines, [OIII]52 line has been challenging to measure for local galaxies and ULIRGs. In particular, Herschel Space Observatory[58] provided far-IR spectroscopy with unprecedented sensitivity and spatial resolution. However, the [OIII]52 μm line lies outside the 55 to 210 μm spectral range of PACS[59] for $z < 0.06$ objects. Herschel completed science operations in May 2013. The SOFIA observatory[60] is now in its full science operations and provides the spectroscopic coverage over the necessary wavelength range for measuring the full far-IR metallicity diagnostic.

We initially selected 11 ULIRGS from HERUS, SHINING, and GOALS surveys, but reduced the sample to 5 ULIRGS that have [OIII]52 μm line uncontaminated by the atmospheric transmission window accessible with SOFIA/FIFI-LS. In the main Letter, we present SOFIA/FIFI-LS observation of these five local ULIRGs with $S_{60\mu m} \geq 7$ Jy at $0.035 < z < 0.075$ which is conducted to obtain missing lines from the full set of [OIII]52 μm, [OIII]88 μm, and [NIII]57 μm lines. These lines are necessary for measuring robust estimates of gas-phase metallicity that are

almost independent of the ionizing source and ionization parameter[54].

2 SOFIA/FIFI-LS Data

FIFI-LS[61] is a far-IR IFU spectroscopy instrument in the mid-IR wavelengths onboard SOFIA, with the design and capabilities similar to those of the Herschel/PACS instrument but with a shorter spectral wavelength cutoff than PACS. In the 51–125 μm blue channel, it has 5 $\times$ 5 spatial pixels (spaxels) of size 6 arcseconds per pixel. We obtained far-IR spectroscopic observations of all our sources from February 2020 to June 2021 during Cycles 8 and 9 of SOFIA operations using the FIFI-LS instrument (PID:08_0095). Our main target line was [OIII]52 μm line as it is not covered by Herschel/PACS data for any of our local sources. However, we also observed [NIII]57 μm line of IRAS 15250+3609 as it is not available with Herschel/PACS in the SHINING archive. All the SOFIA data have gone through the Level 4 pipeline reduction at the SOFIA Science Center. The analysis includes the conversion of raw data to astronomical observations, including astrometry and flux calibrations, as well as corrections for the instrument response and atmospheric transmission.

The Level-4 spectral data cube for each ULRIG was further analyzed for scientific measurements using the Python GUI software SOSPEX[62]. We extract the 1D spectra by integrating the spectral images over an area corresponding to the existing Herschel/PACS observations (Fig. 3). We fit a single Gaussian function to continuum-subtracted spectra centered at the known peak emission of galaxies based on their confirmed redshifts to measure line flux densities and their corresponding uncertainties. We perturb the spectra using their error distributions and estimate the line flux ratio for an hundred trials. The average and standard deviation of hundred trials are adopted as the line flux density and its uncertainty. The line flux maps and continuum-subtracted spectra for all the data are presented in Figure 3. We also plot an ellipse in each line map that shows the region from which the spectrum is extracted.

2.1 Ancillary Data

Herschel/PACS[59] provided the most extensive archive of spectral observations of [NIII] and [OIII] lines. [NIII]57 and [OIII]88 spectra are taken by Herschel/PACS for all our objects except for IRAS 15250+3609. A detailed description of the data reduction and flux measurements of [NIII]57 and [OIII]88 lines can be found in the SHINING data release paper[48]. [NIII]57 line flux of IRAS 15250+3609 is measured from SOFIA/FIFI-LS observations. All the line fluxes for our sample are given in Table 1 of the main letter.

3 Far-IR metallicity

A recent study[48] revisited the mass-metallicity relation of the SHINING (U)LIRGs with metallicities constrained from the [OIII]88/[NIII]57 ratio. They showed that (U)LIRGs tend to

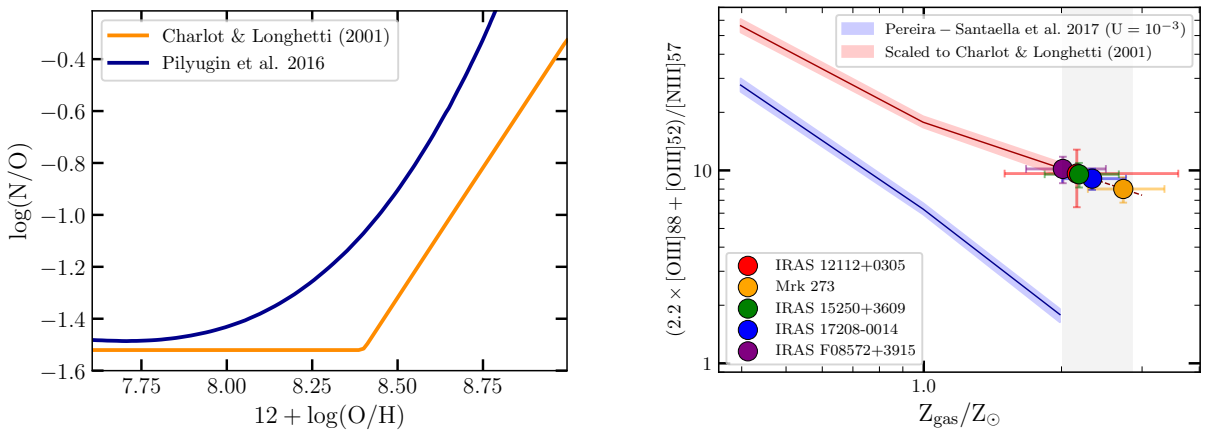

Figure 1 – *Left:* $\mathrm{N/O}$ as a function of $\mathrm{O/H}$. The blue line is a third-order polynomial fit to the observed $\mathrm{N/O}$-$\mathrm{O/H}$ relation[67], which is employed in FIR calibration. The calibration for optical metallicity is based on a relation[66], which is shown with an orange line. The discrepancy between the two models directly affects the metallicity measurements and one needs to correct this systematic offset resulting from different assumptions. *Right:* The blue line shows the FIR metallicity calibration employing observed $\mathrm{N/O}$-$\mathrm{O/H}$ relation (blue line in the left panel), while the red line shows the scaled relation which is corrected for the systematic difference between two $\mathrm{N/O}$-$\mathrm{O/H}$ models. We use the scaled relation to measure the metallicities to maintain comparable results with optical measurements. For the solar metallicity, we adopt $12 + \log(\mathrm{O/H})_{\odot} = 8.69$[75].

lie below the Mass-Metallicity Relation (MZR) of star-forming galaxies, but the offset is smaller than previously thought from studies based on optical-based metallicities. In this paper, for the first time, we use a robust tracer, (2.2×[OIII]88+[OIII]52)/[NIII]57, to measure far-IR metallicities for our ULIRG sample and draw definite conclusions on whether the optical-based metallicities are underestimated thus cannot represent the ULIRG sample. We convert line ratios, (2.2×[OIII]88+[OIII]52)/[NIII]57, to gas-phase metallicity using a calibration introduced by Ref.[54], considering the ionization parameter value of $\mathrm{U} = 10^{-3}$. For our sample with $\Sigma_{\mathrm{FIR}} \sim 10^{11} - 10^{12}$ $\mathrm{L_{\odot}/Kpc^2}$ an ionization parameter of $\mathrm{U} \sim 10^{-2.7} - 10^{-3.5}$ is estimated from observations[49]. This variation has a negligible effect on our metallicity measurements (< 0.05 dex).

To directly compare our results with metal abundances measured for the same ULIRGS with fine structure lines at optical wavelengths[65], we scale our gas-phase metallicity measurements to take into account the differences in the FIR metallicity calibration[54] and optical metallicity calibration[65]. The FIR-based metallicity calibration[54] utilizes an observational relation for $\mathrm{N/O}$ vs $\mathrm{O/H}$ while optical metallicity calibration[65] employs a theoretical model[66] to convert from N/O ratio to O/H estimates. These two relationships, one observational and one from a model, are are shown in Figure 1 of the Methods Section, suggesting that assumptions regarding the behavior of $\mathrm{N/O}$ as a function of $\mathrm{O/H}$ directly affect the metallicity measurements. For FIR metallicity, we scale the calibration[54] to allow a direct comparison with existing optical measurements and the

MZR relation. In effect, we have converted our abundance measurements, first calibrated with the observed relation[54] to that of the model used in SDSS work[65]. (right panel in Figure 1).

Further, we explore whether re-calibrating the metallicities of the FIR can affect our results. We use the original FIR metallicity calibration [54] without scaling it to the theoretical model of $\mathrm{N/O} - \mathrm{O/H}$ relation[66]. Figure 2 shows the comparison of the FIR metallicities derived from original calibration and MZR of SDSS star-forming galaxies [79], which are calculated with the consistent assumption of $\mathrm{N/O} - \mathrm{O/H}$ relation as FIR metallicity. We find that ULIRGs lie on the MZR of star-forming galaxies without any evidence of significant under-abundance, confirming our findings in the main Letter.

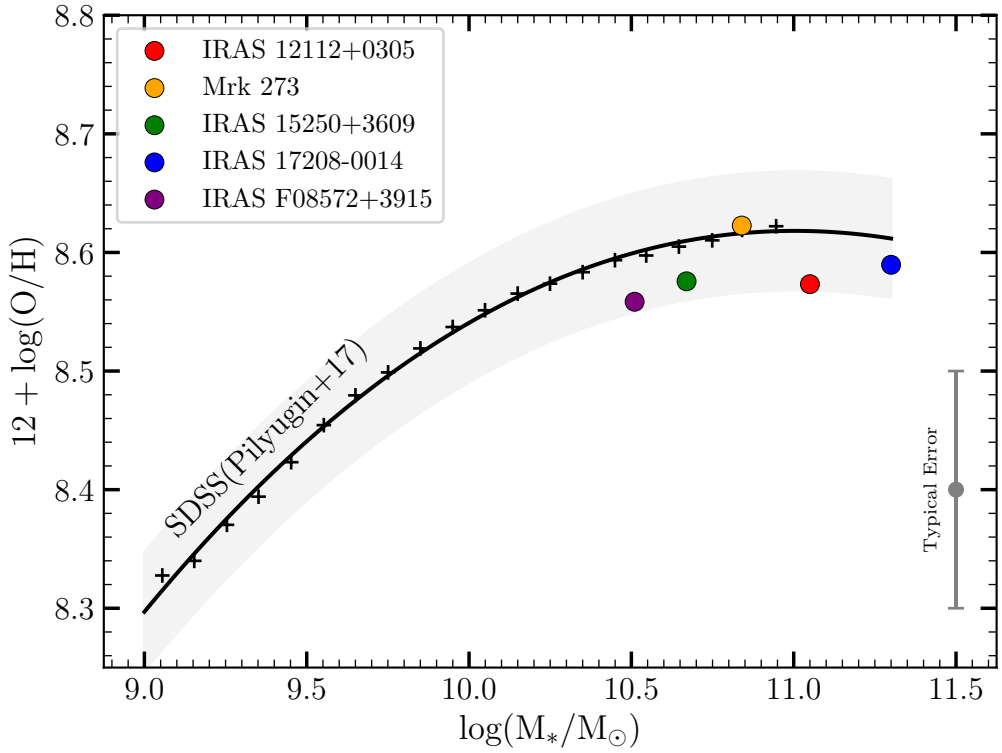

Figure 2 – Similar to Figure 1 of the main Letter, but FIR metallicities are derived from the original calibration without scaling values to the theoretical model of $\mathrm{N/O} - \mathrm{O/H}$ relation. The MZR of SDSS star-forming galaxies is shown from calibration with consistent assumption of $\mathrm{N/O} - \mathrm{O/H}$ relation as FIR metallicity. The plus signs showing the MZR of star forming SDSS galaxies at $z = 0.05$ are taken from literature [79]. The black line is a third-order polynomial fit to SDSS MZR data points.

4 Stellar masses and optical metallicities

In Fig 1 and 2 of the Main Letter, the stellar mass of IRAS 12112+0305, Mrk 273, IRAS 17208-0014, and IRAS F08572+3915 are adopted from the measurements[68] based on the SED fitting of the UV-NIR part of the spectrum. Stellar masses of 15250+3609 and IRAS 17208-0014 are derived from SED fitting over NIR-Radio and UV-Radio part of the spectrum, respectively[69,70]. Our sample consists of galaxies with $10^{10.5}\mathrm{M}_{\odot} < \mathrm{M}_{*} < 10^{11.3}\mathrm{M}_{\odot}$, which are located in the massive end of the MZR.

The optical metallicities of IRAS 15250+3609 and IRAS F08572+3915 are taken from literature and converted to the desired calibration[65] if they are computed using different calibration[71,72]. For the other three sources, we use O3N2=([OIII]5007/Hβ)/([NII]6584/Hα) indicators to estimate the oxygen abundances as all these optical lines are available for IRAS 17208-0014, Mrk 273 and IRAS 12112+0305[73]. All oxygen abundance estimates are converted to the desired calibration[65]. We find that based on optical metallicities, ULIRGs have a significant offset (~ 0.3 dex) from the MZR, which is consistent with previous studies[72]. However, when we use FIR-based gas-phase metallicities, such offset disappears. Previous studies found that luminous optically-selected mergers are under-abundant, $\lesssim 0.1$ dex[74]. Our results imply that ULIRGs follow similar luminous star-forming galaxies and unusual under-abundance (~ 0.3 dex) found in optical metallicities is a result of heavily obscured metal-rich gas which has a negligible effect when using the FIR line diagnostics.

Shown in Figure 2 of the main Letter, we draw a control sample of star-forming galaxies from the MPA/JHU Value-Added Galaxy Catalog of SDSS-DR7[65,77,78] with a similar stellar mass ($10^{10.5}M_{\odot} \lesssim M_{*} \lesssim 10^{11.5}M_{\odot}$) and star formation rate ($\mathrm{SFR} \sim 10^{2.5}$ $\mathrm{M}_{\odot}/\mathrm{year}$) to our ULIRG sample but with a negligible amount of dust ($E(B-V) < 0.06$). We find that these less dusty galaxies have average optical metallicity of 9.1, while the average optical metallicity of our sample is 8.8. One might conclude that the 0.3 dex offset implies that ULIRG sample does not follow the stellar mass-SFR-metallicity relation, known as fundamental metallicity relation[76]. However, optical lines are susceptible to extinction and thus, FIR metallicity calibration provides a reliable measurement for gas-phase metallicity of heavily dust-obscured systems. We find that FIR metallicity measurements of ULIRGs with an average of 9.05 are consistent with the average metallicity of galaxies with similar stellar mass and start formation rate. Therefore, our ULIRG sample follows the fundamental metallicity relation and optical lines are not representative of the metallicity of heavily dust-obscured galaxies.

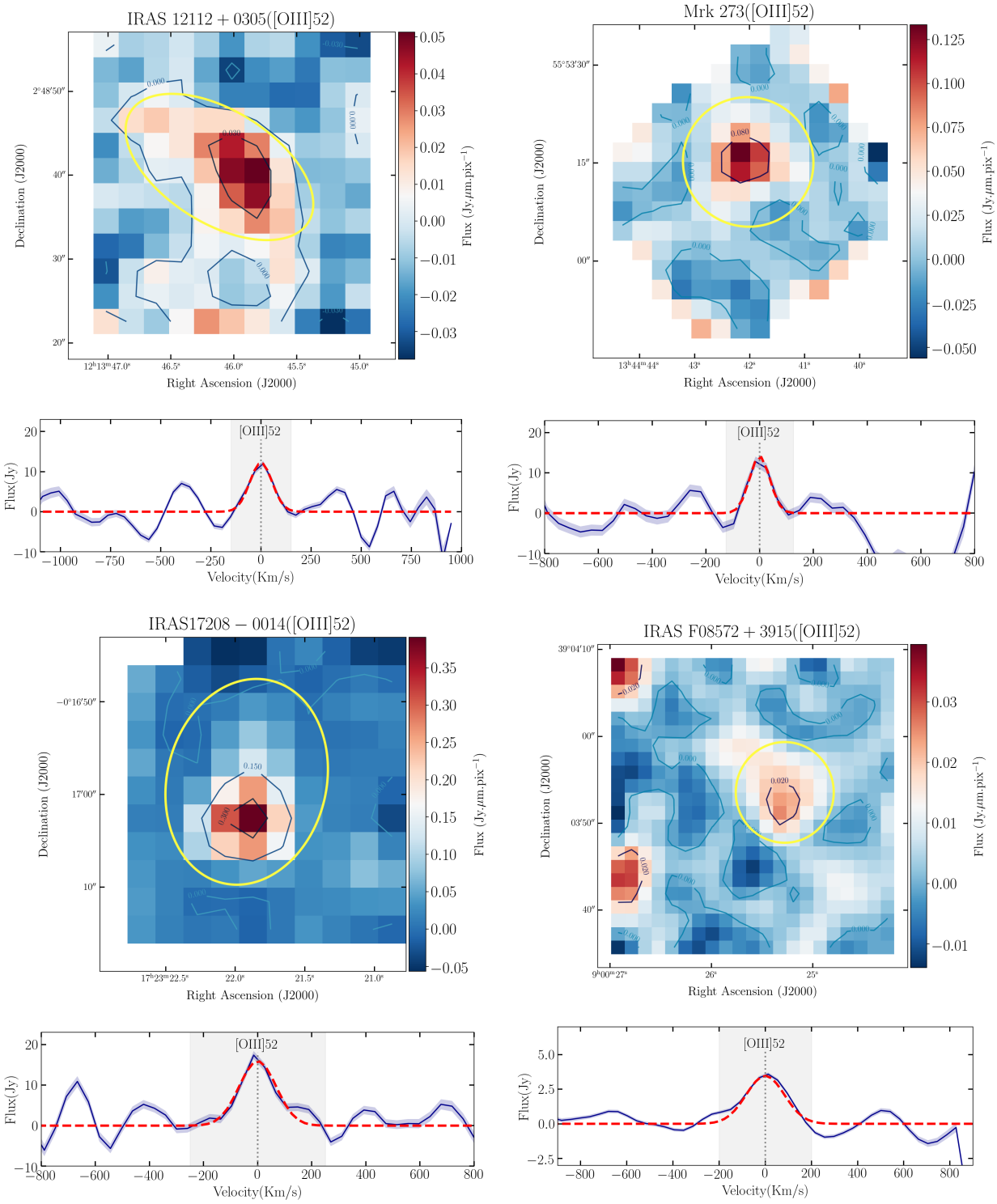

Figure 3 – Line maps and spectra of our sample targeted by SOFIA/FIFI-LS.

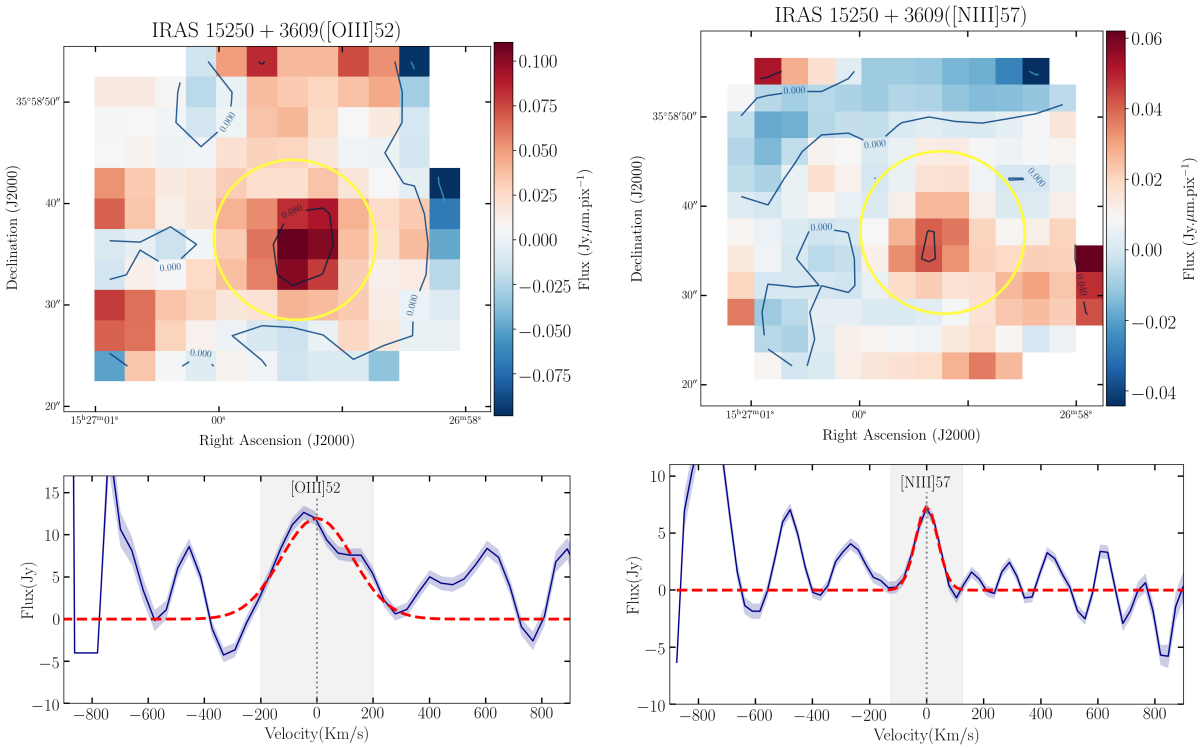

Figure 3 – Continued: Each panel shows the moment 0 map of the spectral line with a yellow ellipse that demonstrates the region over which the spectrum is measured. In the bottom sub-panels, the extracted spectrum is shown along with the best-fit Gaussian function. The blue shaded region around the spectrum corresponds to the 1σ uncertainty of the spectrum. The gray shaded regions on each spectrum show the range of velocity in which the 0^{th} moment line maps are calculated.

Methods References

46. Chabrier, G. Galactic Stellar and Substellar Initial Mass Function. *PASP* **115**, 763–795 (2003).

47. Komatsu, E. *et al.* Seven-year Wilkinson Microwave Anisotropy Probe (WMAP) Observations: Cosmological Interpretation. *Astrophys. J. Supp.* **192**, 18 (2011).

48. Herrera-Camus, R. *et al.* SHINING, A Survey of Far-infrared Lines in Nearby Galaxies. I. Survey Description, Observational Trends, and Line Diagnostics. *Astrophys. J.* **861**, 94 (2018a).

49. Herrera-Camus, R. *et al.* SHINING, A Survey of Far-infrared Lines in Nearby Galaxies. II. Line-deficit Models, AGN Impact, [C II]-SFR Scaling Relations, and Mass-Metallicity Relation in (U)LIRGs. *Astrophys. J.* **861**, 95 (2018b).

50. Sturm, E. *et al.* Massive Molecular Outflows and Negative Feedback in ULIRGs Observed by Herschel-PACS. *Astrophys. J.* **733**, L16 (2011).

51. Díaz-Santos, T. *et al.* A Herschel/PACS Far-infrared Line Emission Survey of Local Luminous Infrared Galaxies. *Astrophys. J.* **846**, 32 (2017).

52. Saunders, W. *et al.* The PSCz catalogue. *Mon. Not. R. Astron. Soc.* **317**, 55–63 (2000).

53. Farrah, D. *et al.* Far-infrared Fine-structure Line Diagnostics of Ultraluminous Infrared Galaxies. *Astrophys. J.* **776**, 38 (2013).

54. Pereira-Santaella, M., Rigopoulou, D., Farrah, D., Lebouteiller, V. & Li, J. Far-infrared metallicity diagnostics: application to local ultraluminous infrared galaxies *Mon. Not. R. Astron. Soc.* **470**, 1218–1232 (2017).

55. Armus, L. *et al.* Observations of Ultraluminous Infrared Galaxies with the Infrared Spectrograph on the Spitzer Space Telescope. II. The IRAS Bright Galaxy Sample. *Astrophys. J.* **656**, 148–167 (2007).

56. Farrah, D. *et al.* High-Resolution Mid-Infrared Spectroscopy of Ultraluminous Infrared Galaxies. *Astrophys. J.* **667**, 149–169 (2007).

57. Desai, V. *et al.* PAH Emission from Ultraluminous Infrared Galaxies. *Astrophys. J.* **669**, 810–820 (2007).

58. Pilbratt, G. L. *et al.* Herschel Space Observatory. An ESA facility for far-infrared and submillimetre astronomy. *Astron. Astrophys.* **518**, L1 (2010).

59. Poglitsch, A. *et al.* The Photodetector Array Camera and Spectrometer (PACS) on the Herschel Space Observatory. *Astron. Astrophys.* **518**, L2 (2010).

60. Temi, P, Hoffman, D, Ennico, K & Le, J SOFIA at Full Operation Capability: Technical Performance. *Journal of Astronomical Instrumentation* **7**, 1840011–186 (2018).

61. Fischer, C. *et al.* FIFI-LS: The Field-Imaging Far-Infrared Line Spectrometer on SOFIA. *Journal of Astronomical Instrumentation* **7**, 1840003–556 (2018).

62. Fadda, D & Chambers, E. T. SOSPEX, an interactive tool to explore SOFIA spectral cubes. *American Astronomical Society Meeting Abstracts* #231 **231**, 150.11 (2018).

63. Liu, X. -W. *et al.* ISO LWS observations of planetary nebula fine-structure lines. *Mon. Not. R. Astron. Soc.* **323**, 343–361 (2001).

64. Nagao, T., Maiolino, R., Marconi, A. & Matsuhara, H. Metallicity diagnostics with infrared fine-structure lines. *Astron. Astrophys.* **526**, A149 (2011).

65. Tremonti, C. A. *et al.* The Origin of the Mass-Metallicity Relation: Insights from 53,000 Star-forming Galaxies in the Sloan Digital Sky Survey. *Astrophys. J.* **613**, 898–913 (2004).

66. Charlot, S. & Longhetti, M. Nebular emission from star-forming galaxies. *Mon. Not. R. Astron. Soc.* **323**, 887–903 (2001).

67. Pilyugin, L. S. & Grebel, E. K. New calibrations for abundance determinations in H II regions. *Mon. Not. R. Astron. Soc.* **457**, 3678–3692 (2016).

68. U, V. *et al.* Spectral Energy Distributions of Local Luminous and Ultraluminous Infrared Galaxies. *Astrophys. J. Supp.* **203**, 9 (2012).

69. da Cunha, E., Charmandaris, V., Díaz-Santos, T., Armus, L., Marshall, J. A. & Elbaz, D. Exploring the physical properties of local star-forming ULIRGs from the ultraviolet to the infrared. *Astron. Astrophys.* **523**, A78 (2010).

70. Vega, O., Clemens, M. S., Bressan, A., Granato, G. L., Silva, L. & Panuzzo, P. Modelling the spectral energy distribution of ULIRGs. II. The energetic environment and the dense interstellar medium. *Astron. Astrophys.* **484**, 631–653 (2008).

71. Monreal-Ibero, A., Colina, L., Arribas, S. & García-Marín, M. Search for tidal dwarf galaxy candidates in a sample of ultraluminous infrared galaxies. *Astron. Astrophys.* **472**, 421–433 (2007).

72. Rupke, D. S. N., Veilleux, S. & Baker, A. J. The Oxygen Abundances of Luminous and Ultraluminous Infrared Galaxies. *Astrophys. J.* **674**, 172–193 (2008).

73. Hou, L. G., Wu, Xue-Bing & Han, J. L. Ultra-luminous Infrared Galaxies in Sloan Digital Sky Survey Data Release 6. *Astrophys. J.* **704**, 789–802 (2009).

74. Kewley, L. J., Geller, M. J. & Barton, E. J. Metallicity and Nuclear Star Formation in Nearby Galaxy Pairs: Evidence for Tidally Induced Gas Flows. *Astron. J.* **131**, 2004–2017 (2006).

75. Asplund, M., Grevesse, N., Sauval, A. J. & Scott, P. The Chemical Composition of the Sun. *ARA&A* **47**, 481–522 (2009).

76. Mannucci, F., Cresci, G., Maiolino, R., Marconi, A. & Gnerucci, A. A fundamental relation between mass, star formation rate and metallicity in local and high-redshift galaxies. *Mon. Not. R. Astron. Soc.* **408**, 2115–2127 (2010).

77. Brinchmann, J. *et al.* The physical properties of star-forming galaxies in the low-redshift Universe. *Mon. Not. R. Astron. Soc.* **351**, 1151–1179 (2004).

78. Kauffmann, G. *et al.* Stellar masses and star formation histories for 10^5 galaxies from the Sloan Digital Sky Survey. *Mon. Not. R. Astron. Soc.* **341**, 33–53 (2003).

79. Pilyugin, L. S., Grebel, E. K., Zinchenko, I. A., Nefedyev, Y. A. & Mattsson, L. On the influence of the environment on galactic chemical abundances. *Mon. Not. R. Astron. Soc.* **465**, 1358–1374 (2017).

5 Data Availability Statement

Data supporting this study is publicly available or will be available by June 2022 through the NASA/IPAC Infrared Science Archive, under Plan ID of 08_0095. Currently, SOFIA/FIFI-LS observations are publicly available for IRAS F08572+3915 and Mrk273 and will be made available for the remainder of the sources by June 2022.